Efficient calculation of the three-dimensional sound pressure field around a railway track

Jannik S. Theyssen*, Astrid Pieringer, Wolfgang Kropp

*Chalmers University of Technology, Division of Applied Acoustics,
Department of Architecture and Civil Engineering, Sven Hultins Gata 8a,
41258 Gothenburg, Sweden*

Abstract

The wavenumber domain Boundary Element method (or 2.5D BE) is well suited for calculating the acoustic sound field around structures with a constant cross-section along one dimension, such as noise barriers or railway track. By expressing the sound field along this dimension in wavenumber domain, the numerical model is reduced from a 3D model to 2D models at each wavenumber. A consequence of the required discrete Fourier domain representation is that the sound field is represented by periodically repeating sections, of which only one section is physically meaningful. The resolution and the number of required wavenumbers increases with the desired length and spatial discretization of this section. Describing the sound field adequately to auralising the sound field without disturbing artefacts requires a large number of wavenumbers (and thus 2D BE computations), which is not feasible for large geometries. Here, a method is introduced that allows the calculation of the 3D sound field by solving a single 2D BE problem for a dense frequency spectrum and interpolating at higher wavenumbers. The calculation efficiency is further increased by pre-calculating the acoustic transfer functions between each BE surface element and receiver positions. Combining these two methods allows the efficient calculation of the 3D sound field. The numerical approach is validated by comparison to a standard 2.5D BEM calculation and an analytical model. Pre-calculated transfer functions to calculate the sound radiation from railway track are presented and made available online.

Keywords: 2.5D BE, Acoustic sound field, Acoustic transfer functions, Numerical methods, Railway track

---

*Corresponding author
   Email address: `jannik.theyssen@gmail.se` (Jannik S. Theyssen)

1. Introduction

With growing transport needs and the intended shift towards more sustainable modes of transport, noise from railroad operations is expected to grow [1]. Rolling noise due to the vibrations in the track and the wheels dominates the total noise in a wide range of vehicle speeds [2]. Estimating the noise radiated from operations on new tracks or the effect of introducing abatement measures on existing tracks has been of interest to both the scientific community and railway operators for several decades. Starting with analytical models, as for example presented by Remington [3], the requirements on and the complexity of such predictive models has continuously grown in parallel to the computational possibilities. Thompson et al. [4] used point-dipole sources to represent the radiation of a rail in free space and researched its directivity. This approach was continued by Zhang et al. [5], where the effect of the discrete support and the proximity to the ground was included using basic line-multipole sources and quadrupoles in each sleeper span.

A prevalent numerical approach for calculating the radiation from the rail is the Wavenumber domain Boundary Element method (WBEM), an adapted Boundary Element method in which one dimension is discretised in wavenumber domain [6, 7, 8, 9, 10, 11]. This has a computational advantage as the large, 3D BE geometries are reduced to 2D BE geometries. These 2D BE problems are then solved for each wavenumber in a spectrum, at each desired frequency. The computational cost rises proportional to the number of 2D BE calculations, which itself depends on the resolution and the upper limit of both spectra. The upper limit is set by the required temporal- and spatial resolution. Nilsson et al. [8] point out that in case of radiation from a rail, whose vibration is typically dominated by few, propagating waves, the wavenumbers can be spaced more closely to these waves to increase the efficiency in the calculation. However still, for other applications and for a desired high spatial and temporal resolution of the sound field, the computational cost of the standard 2.5D method can be infeasible. A high spatial and temporal resolution is necessary when aiming for a time-domain calculation of the sound field quantities. A time-domain approach allows, among others, the calculation of peak-levels, an auralisation of the signal, the calculation of squealing noise amplitudes, and the acoustic effect of a wheel flat or a rail joint or other transients in the rolling noise. The need for developing a time-domain model for the prediction of transient noise has been pointed out by Torstensson et al. [12] and Nielsen et al. [13].

Here, we describe an extension to the WBEM for calculating the 3D sound field generated by the vibrations of railway tracks. This sound field is calculated efficiently in a resolution adequate to for instance modelling a pass-by of a moving force in time-domain. Note that a similar method is used by Li et al. [14] for predicting the low-frequency radiation from concrete bridges. There, the radiation is instead precalculated per bridge mode instead of per BE node, and the analysis is limited to the frequency range up to 1000 Hz. The computational efficiency is addressed in two ways. Firstly, a geometric relation between the wavenumber in air and the wavenumber along the track is used to circum-

vent the need for solving the BE-problem for each combination of wavenumber and frequency. Instead, the BE-problem only needs to be solved for the lowest wavenumber in the spectrum. Then, the BE-result at any higher wavenumber can be derived by an interpolation operation. Essentially, the 3D sound field can be calculated for the cost of a 2D sound field, plus an interpolation operation. This massively reduces the computational cost when using the WBEM. And secondly, acoustic transfer functions are pre-calculated for common acoustic geometries such as a rail in free space and half-space, a rail above a track surface, and a track and train combination. Once accomplished, this replaces the need for solving the BE-problem with a simple multiplication and summation operation. These two approaches are presented in Section 2 and 3, respectively. A validation of the first approach is presented in 2.2. In section 3.2, four acoustic geometries are introduced for which the transfer functions have been pre-calculated. An example of these transfer functions is discussed for illustration. The calculation procedure is made available online in an open-source Python package [15], allowing the calculation of the sound pressure in several points as well as the total radiated sound power for given surface velocity data. The corresponding acoustic transfer functions are available online [16].

2. Calculating the 3D sound field from a 2D solution

This section introduces the first approach of reducing the numerical effort when predicting the 3D sound field generated by track surface vibrations. After introducing the method, a validation is presented.

2.1. Method

The approach to calculating the 3D sound field is based on the WBEM [8]. WBEM is well suited for geometries which are approximately constant in one dimension. The constant geometry in the cross-section allows discretizing the sound field in the wavenumber domain and reduces the 3D BE problem to 2D problems at each wavenumber.

Figure 1 shows the cross-section of a rail located in the y,z-plane, which is assumed to be constant along the x-direction. A wavenumber K_0 in air is indicated by the orange arrow. It can be expressed as the vector sum of the in-plane component α and the component in x-direction κ_0. A second wavenumber K_n is indicated in green, with the same projection on the y,z-plane and a component along the x-direction κ_n. Each combination of frequency (and thus, K) and wavenumber κ in x-direction leads to one 2D BE problem to be solved.

The two-dimensional Helmholtz integral equation for an unbounded exterior problem is

$$C\left(P\right)p\left(P\right) = -\int_{\Gamma}\left(j\omega\rho v_n\Psi + p\frac{\partial\Psi}{\partial n}\right)\mathrm{d}\Gamma \tag{1}$$

in which the integral is evaluated over the boundary Γ, with the density in air ρ, the surface normal velocity v_n, the surface pressure p, and the angular
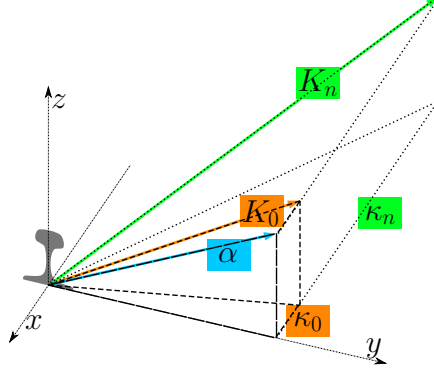
3

Figure 1: Projection of two wavenumbers K_0 and K_n in air on the y,z-plane and the corresponding longitudinal components κ_0 and κ_n, respectively.

frequency $\omega = 2\pi f$. The variable Ψ represents the fundamental solution to the 2D Helmholtz equation at the point P, with

$$\Psi = -\frac{1}{4} H_0^{(2)}(\alpha r) \tag{2}$$

and its derivative in the surface normal direction n,

$$\frac{\partial \Psi}{\partial n} = -\frac{j\alpha}{4} H_1^{(2)}(\alpha r) \frac{\partial r}{\partial n} \tag{3}$$

where $H_0^{(2)}$ is the Hankel function of the second kind and order zero and $H_1^{(2)}$ is of first order. The coefficient $C(P)$ is equal to 1 for P in the acoustic domain and $1/2$ on a smooth boundary. The integral equation is solved on an element-by-element basis by discretization and collocation. A detailed derivation and implementation strategies are, e.g., presented by Wu [17] and left out here for brevity.

The two terms in the Helmholtz integral equation, evaluated on a element-by-element basis, eventually form two matrices (H) and (G) with one column per element and one row per collocation point. These form the global system of equations,

$$\mathbf{C}\vec{p} + \mathbf{H}\vec{p} = \mathbf{G}\vec{V}_n \tag{4}$$

which is sorted according to the known and unknown boundary conditions and solved using a least-square solver if Chief-points are present.

In the standard implementation of this method, this 2D BE problem is be solved for each combination of frequency f and wavenumber κ. The resolution and limits for both the f- and κ-spectrum are chosen based on the desired temporal and spatial limits and resolution. However, this requires solving many 2D BE problems, which is inefficient and, for large geometries, infeasible at high frequencies. Using the relationship between the wavenumber in air and its

projection on the 2D plane for each wavenumber and frequency, this need can be eliminated. For each frequency f there exists one wavenumber in air K

$$K = \frac{2\pi f}{c} \tag{5}$$

which is inversely proportional to the wave speed in air c. As shown in Figure 1, for each wavenumber along the track κ, this wavenumber in air K can be projected on the 2D plane (here, the y,z-plane) by

$$\alpha^2 = K^2 - \kappa^2 \tag{6}$$

which corresponds to projecting K on a component κ along the waveguide and a component α in the 2D cross-section. Notice that the wavenumber in air K and the longitudinal wavenumber κ are independent, as they are a consequence of the chosen discretisation of frequency- and wavenumber domain, respectively. Eq. 6 can instead be written as

$$\alpha^2 = \left(\frac{2\pi f}{c}\right)^2 - \kappa^2 \tag{7}$$

For each combination of κ and wavenumber in air K there is exactly one α in the 2D plane. However, a given α can be the result of infinitely many combinations of κ and K. Figure 1 shows two combinations of κ and K (κ_0, K_0 and κ_n, K_n) which share the same α. This is true if

$$K_0^2 - \kappa_0^2 = K_n^2 - \kappa_n^2 \tag{8}$$

or, using Eq. 5 and rearranging for f_0,

$$f_0 = \sqrt{f_n^2 - \frac{\left(\kappa_n^2 - \kappa_0^2\right) c^2}{\left(2\pi\right)^2}}. \tag{9}$$

This relation can be utilised by first evaluating Eq. 4 for a dense frequency spectrum in combination with a small wavenumber κ_0. Then, for higher wavenumbers κ_n, Eq. 9 maps any frequency to a frequency in the dense original spectrum at which the α in the 2D plane is identical. The calculated frequency f_0 is likely not part of the pre-calculated dense spectrum, and an interpolation operation in frequency domain is necessary. In other words, at each wavenumber except the lowest wavenumber, the operation of solving the 2D BE problem for each frequency in the spectrum can be replaced by a complex interpolation operation. Note that a dense original frequency spectrum is always recommended using this method, even when evaluating only at a few frequency lines per octave band, as Eq. 9 non-linearly maps to frequency lines in between the original ones. A standard implementation of the complex quadratic interpolation is used, interpolating the real and imaginary part seperately (see, e.g., `interp1` in MATLAB or `interp` in Numpy).

To avoid extrapolation, any query point at which to evaluate the interpolation needs to lie between the limits of the original spectrum. Luckily, this requirement is already fulfilled by the method itself. Figure 2 visualises the relation between f_n and f_0 for whole wavenumbers from 0 rad/m to 10 rad/m in the frequency range 0 Hz to 1000 Hz. From Eq. 9 follows that for $\kappa_n > \kappa_0$,
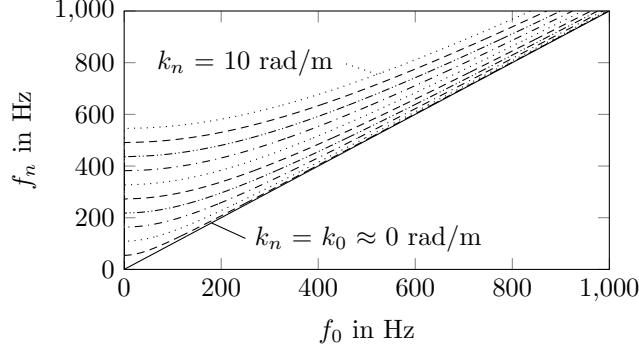

Figure 2: Mapping between f_n and f_0 for selected whole wavenumbers k_n 0 rad/m to 10 rad/m.

the frequency f_0 is strictly smaller than a frequency f_n with the same α in the 2D plane. Therefore, a frequency spectrum at any higher wavenumber maps to smaller frequency lines and thus the upper bound is fulfilled. The lower bound is limited by the physical properties of sound radiation. Figure 2 shows that for increasing wavenumbers, increasing frequencies get mapped to 0 Hz in the f_0 spectrum. Physically, this is because for these combinations of k_n and K_n, the wavenumber in air is smaller than the wavenumber along the track, and so no projection on the 2D plane is possible. Mathematically, this is a consequence of the expression under the root in Eq. 9, which becomes negative for

$$\left(\frac{2\pi f_n}{c}\right)^2 < \kappa_n^2 - \kappa_0^2 \tag{10}$$

which for $k_0^2 \ll k_n^2$ can not be fulfilled for real κ. For imaginary wavenumbers κ, only radiation into near-field occurs, and no sound power is radiated. These wavenumbers are excluded from further calculations.

The method described above establishes a relationship between a given α and combinations of κ and K. For a given α, the phase relation between all source elements and receiver points in the BE formulation is set. However, there is a relevant frequency dependent scaling of the magnitude in the two-dimensional Helmholtz integral equation (Eq. 1), as the first term in the integral contains the factor $j\omega$ and the normal velocity v_n. A scaling of the boundary element equation 4 is proposed,

$$\mathbf{C}\vec{p} + \mathbf{H}\vec{p} = \mathbf{G}^*\vec{V}_n^* = \frac{\mathbf{G}}{j\omega}\vec{V}_n j\omega \tag{11}$$

such that the frequency dependency is instead included in the normal velocity.

The scaling of $\vec{V}_n^*$ can be introduced before or after the solution of the BE problem. The scaling does not affect the type of boundary conditions that can be used. If boundary conditions other than the Neumann boundary condition are used, the elements in the result vector corresponding to a normal velocity need to be scaled accordingly.

In summary, the 3D sound field of a structure with constant cross-section can be calculated in frequency-wavenumber domain by

1. describing the acoustic boundaries and -domain by standard 2D boundary elements
2. selecting an appropriate discretization of the wavenumber and frequency domain
3. solving the 2D BE problem for each frequency in the selected spectrum at the lowest wavenumber in the spectrum k_0
4. for each larger wavenumber k_n,
    (a) calculating the frequency f_0 in the original spectrum that shares the projection of K on the cross-section according to Eq. 9
    (b) interpolating the original spectrum at f_0
    (c) scaling the result according to Eq. 11.

To conclude, this first approach makes it possible to solve the 2D BE problem for only one wavenumber at every frequency in a dense frequency spectrum, and then generates solutions at higher wavenumbers by interpolation and frequency-dependent magnitude scaling of the result.

2.2. Validation of the method

To investigate the validity of the described modelling approach, comparisons to the standard WBEM and an analytical solution for the case of a breathing cylinder are carried out. Figure 3 presents the cross-section of the geometry. The analytical model is based on a breathing line source, located at $(0.5, 0.5)$ m. Assuming a unit presure excitation, the pressure produced by this source at any location in the field is given by

$$p = -\frac{j}{4}\hat{p}H_0^{(2)}(\alpha r) \tag{12}$$

where r describes the distance between source and receiver and $\hat{p} = 1\ Pa$.

The radiating surface in the WBEM model consists of a cylinder with 1 m radius centred at $(0,0)$ m, enclosing the line source. Its surface normal velocity at each element of this cylinder V_n is prescribed such that it matches the velocity in the sound field created by the breathing cylinder.

$$V_n = \frac{\alpha}{4\omega\rho}H_1^{(2)}(\alpha r)\frac{\partial r}{\partial n} \tag{13}$$

where r is the distance from the breathing line source to the element, n is the unit normal vector on the boundary. This way, the pressure on and outside of the
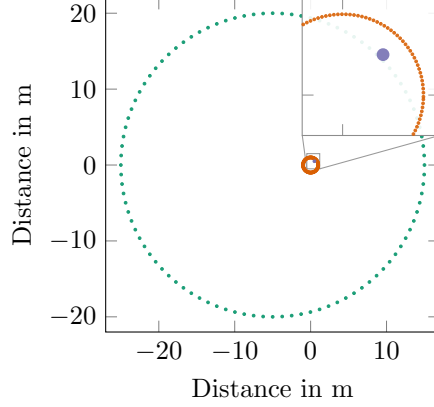
7

Figure 3: Cross-section of the setup for the validation calculation. The thick blue dot marks the location of the line source. The smaller, orange circle represents the surface of the WBE structure while the larger, green circle of points are positions at which the sound pressure is evaluated.

surface of the cylinder should be identical up to numerical accuracy and within the general limitations of the boundary element method. Finally, the WBE model is used to solve the 2D BE problem described in Eq. 1 for $\kappa_0 = 1$ μ rad/m and a frequency spectrum from 0 Hz to 1000 Hz and a resolution of 2 Hz. The sound pressure on the surface and in the field at other wavenumbers is then calculated using the method introduced above.

Frequency spectra of the sound pressure are calculated for three wavenumbers at 120 receiver points which are arranged in a circle with 20 m radius centred at $(-5, 0)$ m. Firstly, the sound pressure at one such receiver is compared for all three methods in Figure 4. The three models produce very similar
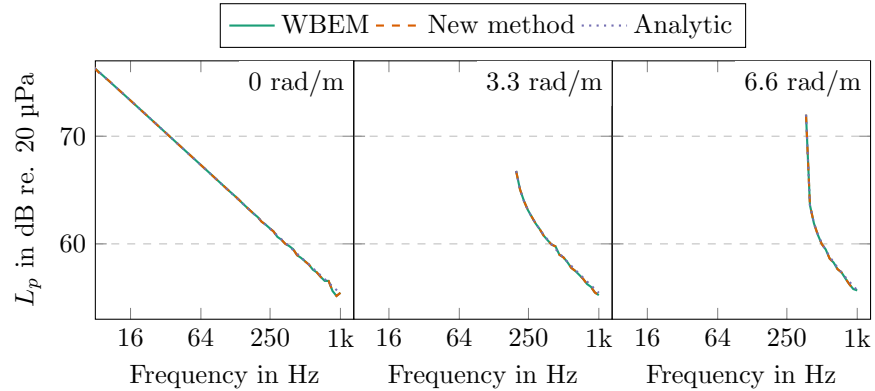

Figure 4: Calculated field point pressure at one field point. The wavenumber κ along the structure is given in the top right corner.

results. The effect of the cut-on frequency at higher wavenumbers is visible for $\kappa = 3.3$ rad/m and $\kappa = 6.6$ rad/m, as no radiation into the far field occurs below 182 Hz and 364 Hz, respectively.

In a second step, the WBEM calculation and the presented method are compared to the analytical model. Figure 5 presents the mean error of each receiver point. Both methods predict the analytical result with high accuracy. A decreasing accuracy with increasing frequency is expected due to the resolution of the BE mesh, which is observed for both methods. Once can conclude that the
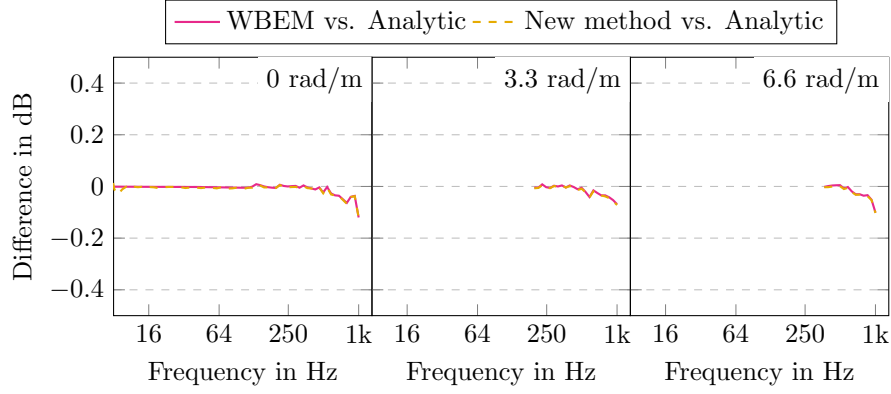
Figure 5: Comparison of the mean difference at all field points.

suggested approach is a suitable extension to the WBEM when dense frequency and wavenumber spectra are calculated.

3. Pre-calculation of the acoustic transfer functions

This section presents the second of two approaches to increasing the computational efficiency for predicting the sound field radiated from railway track vibrations. This is achieved by calculating transfer functions that can be reused in different vibration situations. After this method is introduced below, four geometries are described for which these transfer functions have been evaluated.

3.1. Method

For solving the BE problem, either the pressure, the velocity, or the impedance at each boundary node needs to be prescribed. If no back-coupling between the air and the structure occurs (the radiation impedance in air has a negligible effect on the vibration of the structure), the surface normal velocity can be calculated independently of the boundary element problem. Using the algorithm in Section 2.1 to calculate the radiation for one resulting boundary normal velocity is a significant improvement compared to the standard implementation. However, often several calculation cases need to be solved that share their acoustic geometry but use different normal velocities as the input. This is relevant for

9

example when evaluating the radiation from the track for different excitation positions on the rail, changing track parameters, or altering the the surface roughness of the rail in a wheel pass-by simulation. Based on this, the following discussion is limited to changing the Neumann boundary condition.

Acoustic transfer functions can be pre-calculated by taking advantage of the integral nature of the boundary element formulation. The linear equation system 11 becomes

$$\mathbf{A}\vec{p} = \mathbf{G}^{*}\vec{V}_{n}^{*} \tag{14}$$

when combining the $\mathbf{C}$ and $\mathbf{H}$ matrices into the $\mathbf{A}$ matrix. In this discretized problem formulation, the sound pressure at any receiver position is the sum of the contributions of each source element. The contribution of each source element in turn consists of an acoustic transfer function, scaled with the surface normal velocity of this source element.

The acoustic transfer functions from one source element are calculated by setting its surface normal velocity to 1 m/s and 0 m/s otherwise in $\vec{V}_{n}^{*}$. Solving Eq. 14 for one such case produces transfer functions to all receiver points. However, a complete solution requires solving the large, potentially over-determined and dense matrix system once for every source element. This is a significant initial computational effort. Especially when investigating the radiation from a railway track, the total number of elements can be large when including a train or noise barriers in the geometry. Nonetheless, often only a small part of the geometry actually contributes to the radiation in the calculation, such as the rail and parts of the track surface. These are described by just a fraction of the total number of boundary nodes, and so the pre-calculation can be limited to these areas. Examples for which acoustic transfer functions have been evaluated are described below.

3.2. Description of the pre-calculated transfer functions

The second approach introduced above relies on pre-calculated transfer functions which describe the sound pressure produced in a set of receiver points for a unit normal velocity at the vibrating surface nodes of the structure. These transfer functions have been pre-calculated for four geometries, sketched in Figure 6. The geometries are (a) a UIC 60 rail in free space, (b) the same rail 5 cm above an infinite, acoustically hard surface, (c) the same rail 5 cm above a flat structure which itself is positioned above an infinite, acoustically hard surface, and (d) the rail and track structure below the simplified hull of a passenger train. The track surface is centred laterally while the rail located at the position of the right rail for a standard gauge of 1.435 m. Figure 7 shows the setup used in geometry (d). The other geometries can be derived by removing the respective components. All surface nodes, field points and CHIEF-points used in the calculation are presented in the figure. The surface nodes for which the transfer functions have been calculated are indicated in green. Other (passive) surface nodes are colored blue. All surface nodes are spaced with 7.5 mm to achieve 6 elements per wavelength up to 7.5 kHz. Figure 7c shows the surface
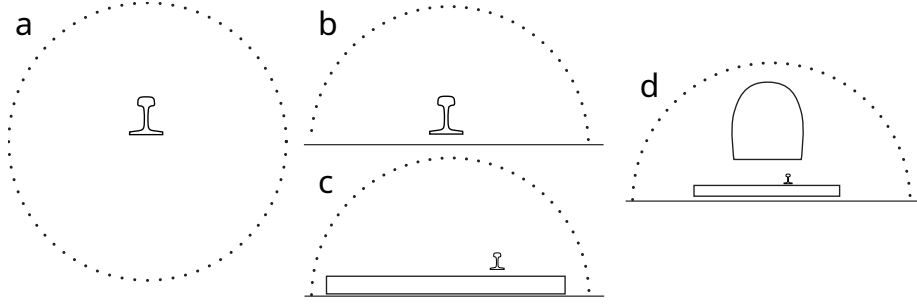
Figure 6: Boundary element geometries for which the acoustic transfer-functions were pre-calculated.

normal direction for each active surface node on the rail and on the surface below.

A total of 21 CHIEF-points are distributed in the rail-, the track- and the train-cross section. Chief points are marked with a red 'X'. The black dots represent receiver positions or 'field points'. In addition to the pass-by measurement positions defined in the standard ISO 3095, four half-circles of points around the track centre with radii 2.5 m, 5 m, 10 m and 20 m and one half-circle with radius 1.2 m centered at the rail. Additional points are included depending on the geometry. More detailed information can be found in the online resources [15, 16]. The additional positions are included to provide a higher flexibility for microphone positioning when for example using the transfer functions for a comparison to measurements.

The pre-calculated transfer functions describe the sound pressure created by each source element on all surface and field nodes, for wavenumber $\kappa_0 = 10^{-6}$ rad/m and a frequency spectrum with 1 Hz resolution up to 7.5 kHz. As an example, the transfer functions corresponding to geometry (a) are investigated in the following, focussing specifically on the transfer functions from the 92 source nodes on the rail surface to 100 receiver points located in a circle with 20 m radius around the rail. The data is three-dimensional (92 x 100 x n_f), where n_f is the number of frequency lines in the pre-calculated spectrum. The transfer functions are therefore only visualised for selected frequencies. Figure 8 demonstrates how the transfer functions are visualised in the following. Each row in the surface plot describes the contribution of a unit normal velocity at one source node to all receiver points. The position of the source nodes on the rail surface is indicated by the gray lines. Analogously, the position of the receivers is indicated by the gray lines below the 2D plot. The color range is adjusted to cover a 20 dB sound pressure level range, normalized with the largest sound pressure level at any receiver node at that frequency. In the selected example, a diagonal trend is visible, indicating that in general, a surface velocity on the left side of the rail contributes mainly to the receiver points on its left side, and so on. At the vertical line marking 90 °, the radiation is almost entirely dominated by the right side of the rail. Large parts of the rail surface, with the
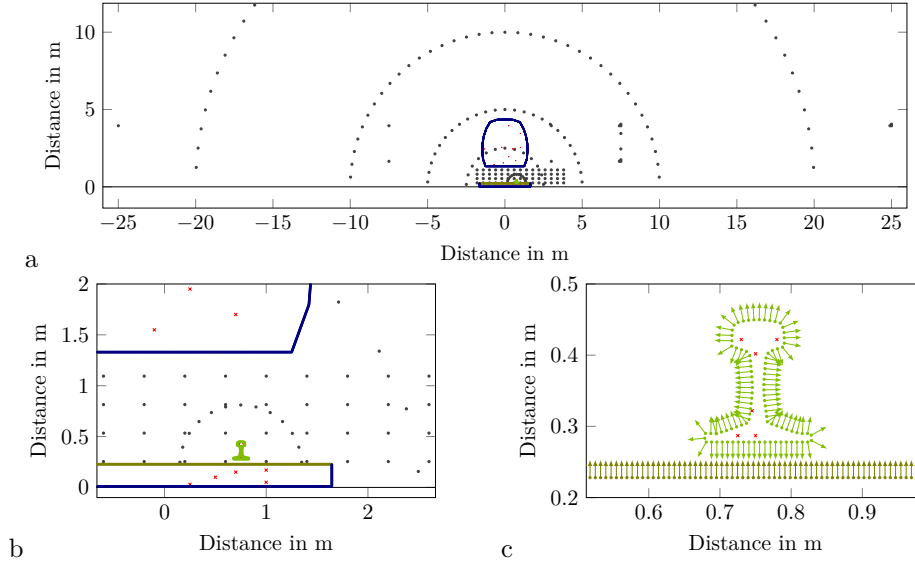
Figure 7: Setup (iv) for which the acoustic transfer functions were evaluated.

exception of the rail foot and the part below the rail head, contribute to the sound pressure in vertical direction.

Figure 9 shows analogous 2D plots for five other frequencies. A distinct interference pattern is visible. Note that the pattern does not arise from the interaction of several sources but instead from the wave field created by a single source and the reflections on the acoustically hard rail surface. Below 500 Hz, the wavelength in air is large compared to the dimensions of the rail. Therefore, the rail geometry does not significantly influence the radiation pattern, and the transfer function of all surface nodes to all receiver points is similar, i.e., the dynamic range of the 2D plot is low. With increasing frequency, the geometry of the rail becomes more influential and the dynamic range gets larger. Distinct squares are visible at locations corresponding to the side of the rail. This can be interpreted such that a vibration in any part of this concave rail section focusses the radiation towards lateral receiver positions. A lateral bending wave would thus produce a dipole-characteristic, in which each lobe is produced by the vibration on the corresponding side of the rail.

A comparable analysis can be carried out using the rail surface nodes themselves as the receiver points. This is shown in Figure 10. The source node is expectedly the main contributor to the sound pressure at its position (thus the diagonal line) A surface velocity in the concave section produces comparatively high pressure at other nodes in the concave section. Again, a frequency dependent interference pattern can be observed.

To calculate the total radiated sound pressure produced by a vibrating rail, each transfer function needs to be multiplied with the corresponding surface vibration. The result is a vector of complex pressures describing the individ-
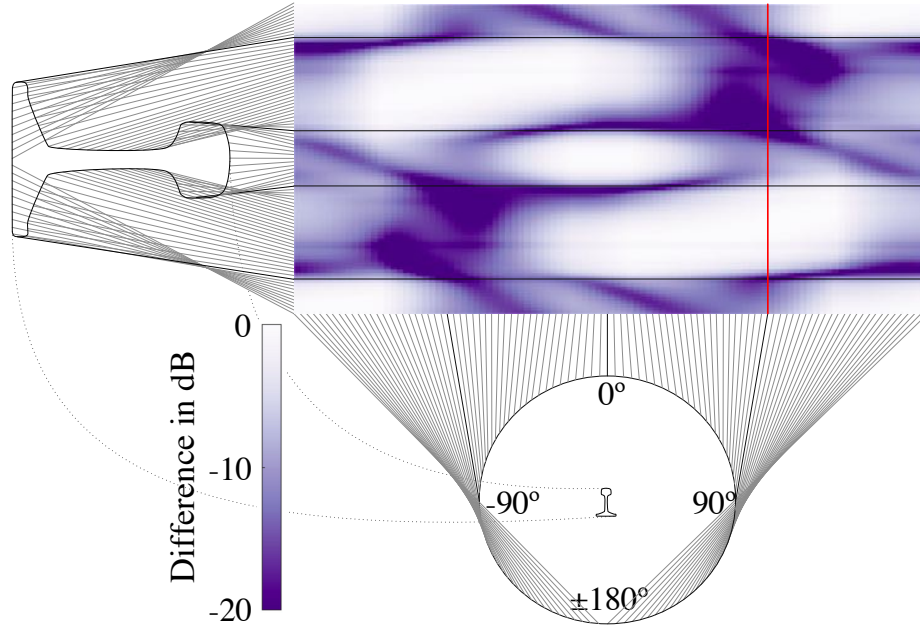
Figure 8: Transfer function magnitude between each source element on the rail and receiver point in a circle with 20 m radius around the the rail. The displayed transfer functions are calculated at 1100 Hz, which is typically close to the pinned-pinned frequency.

ual contributions of each surface section to a receiver point. The sum over these complex pressures is equivalent to the Rayleigh integral over the radiating surface. The application of this method is not the focus of this article.
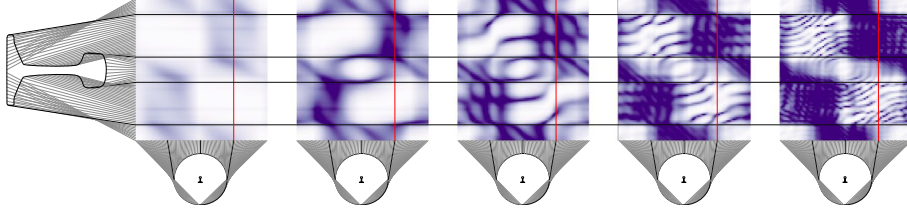
Figure 9: Transfer function from surface velocity on each individual node on the rail surface (y-axis) to the sound pressure in a circle around the rail (x-axis), displayed as the relative difference to the largest contribution, in dB. Left to right: 500 Hz, 1000 Hz, 2000 Hz, 4000 Hz, and 7500 Hz. The receiver angle zero degrees corresponds to a position vertically above the rail and increasing numbers indicate clockwise rotation.
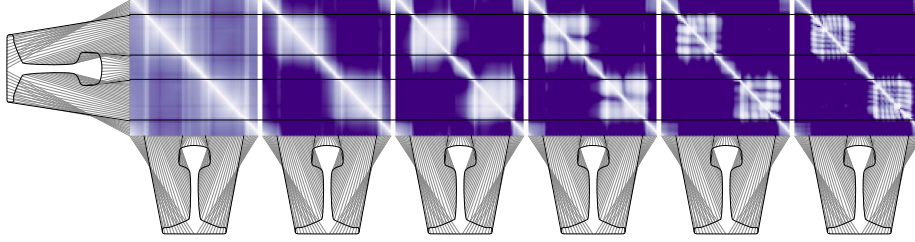

Figure 10: Transfer function from the velocity at each individual surface node (y-axis) to the sound pressure at each surface nodes (x-axis), displayed as the relative difference to the largest contribution, in dB. Left to right: 25 Hz, 500 Hz, 1000 Hz, 2000 Hz, 4000 Hz, and 7500 Hz.

4. Results and applications

This section presents a few considerations regarding the computational efficiency and presents some example applications of the modelling approach.

4.1. Efficiency considerations

The first approach addresses the necessary number of 2D BE solutions. The necessary computing time for one such solution depends on the considered geometry and the available computing resources. Nevertheless, the gained efficiency can be estimated by considering the number of BE solutions.

To produce impulse responses at regularly spaced positions along the track, a regular grid in frequency- and wavenumber domain is a consequence of the discrete Fourier transform. This is illustrated in the following example, in which impulse responses of $T = 1$ s length with a sampling frequency of $f_s = 15$ kHz are desired. Further, the spatial resolution along the track should be such that a vehicle moving at $v = 180$ km/h travels one spatial sample in each time step, i.e, $dx = v \, dt$. The resolution in frequency domain is given by $df = 1/T = 1$ Hz, and analogously, the resolution in wavenumber domain is given by $d\kappa = 2\pi/X_{\mathrm{max}}$. The upper limit of the relevant wavenumber grid is either given by $\kappa_s = 2\pi/dx$, or by κ_{air}, the wavenumber in air. Such a regular grid is presented in Figure 11,
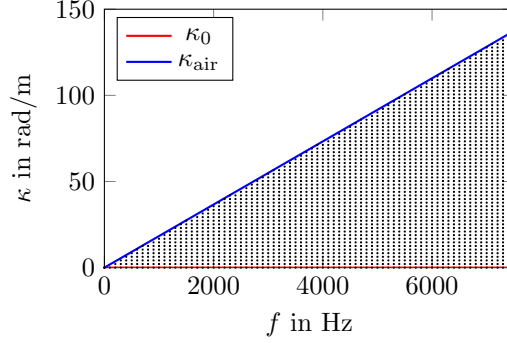
14

Figure 11: Illustration of combinations of wavenumber and frequency at which a 2D BE solution is necessary to produce a regular grid in time- and spatial domain.

in which also k_{air} and k_0 are indicated. The presented grid is sparser than necessary to aid in presentation.

In the presented case and the standard approach, every black dot in Figure 11 represents a 2D BE solution. The approach presented in Section 2.1 requires the calculation of the cases along the red line with a high frequency resolution, after which all other cases can be derived via interpolation. This gain in efficiency is largest if many such 2D BE solutions are necessary, i.e., if the wavenumber resolution is high. This, in turn, is the case if the maximum required distance X_{max} is large. Figure 12 presents the count of the necessary 2D BE solutions over this distance X_{max}. All other parameters are as described above. The 1 Hz resolution of the frequency spectrum leads to 7501 BE problems to be solved in the new approach. If all combinations were to be solved, the computational effort would be several magnitudes higher for $X_{max} > 10$.
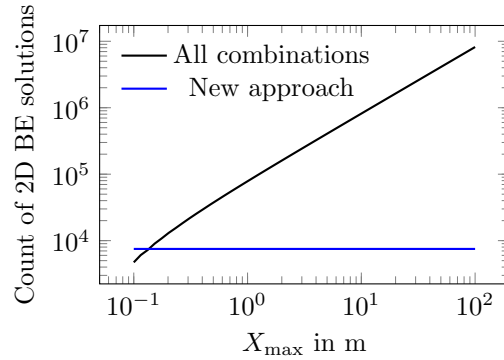

Figure 12: Number of computations necessary when evaluating all grid points or only the dense frequency spectrum at k_0, depending on the maximum distance of interest.

The benefit of pre-calculating the acoustic transfer functions as described in

the second approach is easier to estimate. Initially, a 2D BE problem needs to be solved for each source node (and each frequency and wavenumber!). Once these transfer functions are available, the sound field can be calculated at a comparatively small cost. The pre-calculation is worth the effort as soon as the transfer functions are re-used more often than the number of source nodes in the geometry.

4.2. Application examples

To exemplify possible applications of the presented calculation approach, the sound field radiated by one railway rail is briefly demonstrated in in the following. The transfer functions calculated for setup c (rail above a track, see Figure 6) are used in this example.

The surface vibrations of the rail are calculated using a discretely supported UIC60 rail based on the waveguide Finite Element (WFE or 2.5D FE) method. The WFE approach is not further described, but more details can be found in literature [8, 18, 19]. The WFE method allows calculating the surface normal velocity in three dimensions. The rail is coupled to a spring-mass-spring system in each rail seat. A harmonic unit force excitation is applied on the rail at the location $x = 0$ m. The force is introduced vertically, but slightly off-cenre on the rail head, so that lateral and vertical motion is excited in the rail.
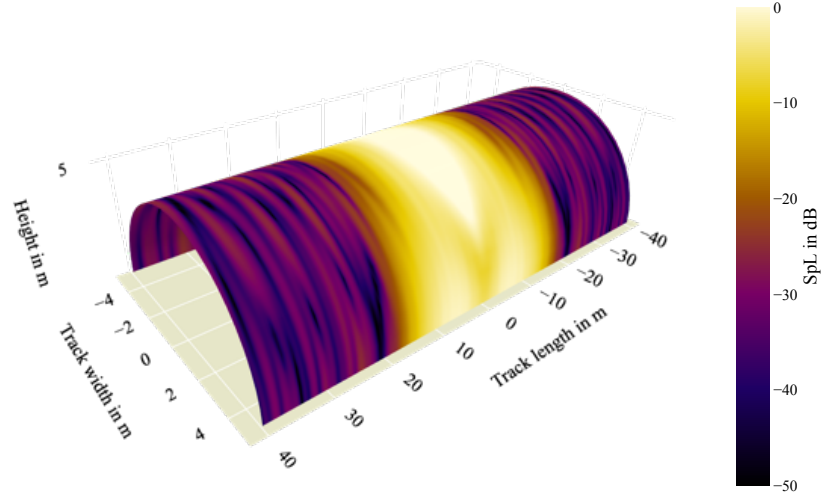

Figure 13: Normalized sound pressure level distribution on a half-cylinder with 5 m radius around the track created by a vibrating UIC60 rail. The rail is excited vertically by a harmonic unit force at 120 Hz.

Figure 13 shows the normalized sound pressure level distribution on a half-cylinder with 5 m radius around the track centre for an excitation at 120 Hz. It is visible that a section of about 20 m produces the largest sound pressure levels in the top 10 dB range. The largest pressure levels are located vertically

above the excitation position, likely due to the mostly vertical motion of the rail. In lateral direction, there are instead two peaks at a distance of about 5 m from the excitation position. The different radiation directivity along the rail is due to the radiation from bending waves. The frequency 120 Hz is below the cut-on frequency of vertical bending waves for this setup, and so only radiation into the near field occurs. The bending stiffness in lateral direction is lower, and so is the cut-on frequency for lateral bending waves. As a result, the sound is radiated at an angle from the excitation point and arrives on the half-cylinder at the observed distance.
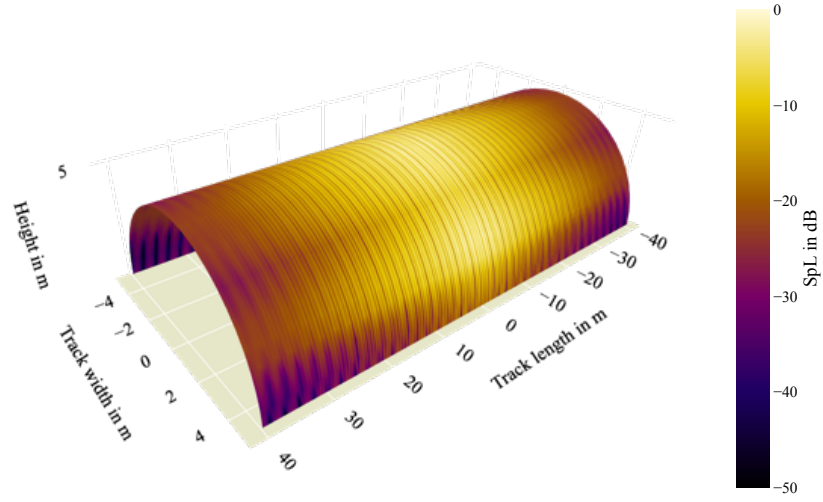

Figure 14: Normalized sound pressure level distribution on a half-cylinder with 5 m radius around the track created by a vibrating UIC60 rail. The rail is excited vertically by a harmonic unit force at the pinned-pinned resonance 1170 Hz.

Figure 14 presents the same setup, but for a different excitation frequency. Here, the system is excited at 1070 Hz, which is close to the pinned-pinned frequency of the rail. The bending waves in the rail can thus travel almost unobstructed and the sound pressure level is accordingly quite similar over a long distance. The sound pressure level in lateral direction is comparatively low as the vertical vibration dominates the sound radiation.

5. Discussion and Conclusion

Two approaches for significantly reducing the effort required to predict the 3D sound field radiated by railway track vibration have been presented, both based on the WBEM (2.5D BEM). In the standard WBEM, a 2D BE problem needs to be solved for each combination of wavenumber and frequency for a given surface velocity.

The first approach avoids the need to solve this BE problem for every combination of wavenumber and frequency by employing a geometric relation between wavenumbers at different frequencies. This effectively creates a 3D description of the sound field for the cost of solving a 2D solution plus an interpolation. The first approach is limited to sound radiation into the far field. This approximation is often used, as only the far-field radiation contributes to the radiated sound power (see, e.g., [8]). A perhaps more significant limitation of the method is that this far, only acoustically hard surfaces are considered. The inclusion of possibly direction-dependent absorption as a boundary condition deserves further thought but is outside the scope of this work. The primary goal of this method is to calculate the sound radiation from slab tracks, for which most surfaces in direct proximity to the rail can be modelled acoustically hard.

The second approach reduces the computational cost when the sound field is predicted for several different cases of structural vibration. By pre-calculating acoustic transfer functions for common geometries, these transfer functions can be re-used. The complex sound pressure at a receiver position can then be calculated by scaling these transfer functions with the corresponding surface velocity and summing over all surface nodes. No BE solution is necessary. The acoustic transfer functions for four such acoustic geometries have been presented.

Combining the two proposed approaches has the potential to describe the sound field created by a railway track with arbitrary resolution in spatial domain, at a massively reduced computational cost compared to 3D Boundary Element formulations and even the standard WBEM. An efficient calculation of the railway track radiation is a prerequisite for physically modelling the pass-by noise generated by a force moving on a rail. The calculation procedure and pre-calculated acoustic transfer functions are documented and made available online in an open-source Python package [15, 16].

References

[1] Railway Noise in Europe, State-of-the-art report, International Union of Railways, 2021.

[2] D. J. Thompson, Railway noise and vibration: mechanisms, modelling and means of control, 1st Edition, Elsevier, Amsterdam ; Boston, 2009.

[3] P. Remington, Wheel/rail noise—Part IV: Rolling noise, Journal of Sound and Vibration 46 (3) (1976) 419–436.

[4] D. J. Thompson, C. J. C. Jones, N. Turner, Investigation into the validity of two-dimensional models for sound radiation from waves in rails, The Journal of the Acoustical Society of America 113 (4) (2003) 1965–1974.

[5] X. Zhang, D. Thompson, E. Quaranta, G. Squicciarini, An engineering model for the prediction of the sound radiation from a railway track, Journal of Sound and Vibration 461 (2019) 114921.

[6] D. Duhamel, EFFICIENT CALCULATION OF THE THREE-DIMENSIONAL SOUND PRESSURE FIELD AROUND A NOISE BARRIER, Journal of Sound and Vibration 197 (5) (1996) 547–571.

[7] M. Hornikx, J. Forssén, The 2.5-dimensional equivalent sources method for directly exposed and shielded urban canyons, The Journal of the Acoustical Society of America 122 (5) (2007) 2532.

[8] C.-M. Nilsson, C. Jones, D. Thompson, J. Ryue, A waveguide finite element and boundary element approach to calculating the sound radiated by railway and tram rails, Journal of Sound and Vibration 321 (3-5) (2009) 813–836.

[9] B. van der Aa, J. Forssén, The 2.5D MST for sound propagation through an array of acoustically rigid cylinders perpendicular to an impedance surface, Journal of Physics D: Applied Physics 48 (29) (2015) 295501.

[10] H. Li, D. Thompson, G. Squicciarini, X. Liu, M. Rissmann, F. D. Denia, J. Giner-Navarro, Using a 2.5D boundary element model to predict the sound distribution on train external surfaces due to rolling noise, Journal of Sound and Vibration 486 (2020) 115599.

[11] J. S. Theyssen, A. Pieringer, W. Kropp, The Influence of Track Parameters on the Sound Radiation from Slab Tracks, in: G. D. et al. (Ed.), Noise and Vibration Mitigation for Rail Transportation Systems, Notes on Numerical Fluid Mechanics and Multidisciplinary Design, Springer International Publishing, Cham, 2021, pp. 90–97.

[12] P. Torstensson, G. Squicciarini, M. Krüger, B. Pålsson, J. Nielsen, D. Thompson, Wheel–rail impact loads and noise generated at railway crossings – Influence of vehicle speed and crossing dip angle, Journal of Sound and Vibration 456 (2019) 119–136.

[13] J. C. O. Nielsen, A. Pieringer, D. J. Thompson, P. T. Torstensson, Wheel–Rail Impact Loads, Noise and Vibration: A Review of Excitation Mechanisms, Prediction Methods and Mitigation Measures, in: G. D. et al. (Ed.), Noise and Vibration Mitigation for Rail Transportation Systems, Vol. 150, Springer International Publishing, Cham, 2021, pp. 3–40.

[14] Q. Li, X. Song, D. Wu, A 2.5-dimensional method for the prediction of structure-borne low-frequency noise from concrete rail transit bridges, The Journal of the Acoustical Society of America 135 (5) (2014) 2718–2726.

[15] J. Theyssen, RailRad - calculate the acoustic radiation from railway track using pre-calculated transfer functions.
URL https://github.com/janniktheyssen/railrad

[16] J. Theyssen, Database for railrad calculation method for simulating sound radiated by railway track vibrations, Dataset Version 1.0.0, Chalmers University of Technology (2022). doi:10.5281/zenodo.6772099.
URL http://www.zenodo.org/6772099

[17] T. W. Wu, Boundary Element Acoustics, no. 7 in Advances in Boundary Elements, 2000.

[18] X. Zhang, D. J. Thompson, Q. Li, D. Kostovasilis, M. G. Toward, G. Squicciarini, J. Ryue, A model of a discretely supported railway track based on a 2.5D finite element approach, Journal of Sound and Vibration 438 (2019) 153–174.

[19] J. S. Theyssen, E. Aggestam, S. Zhu, J. C. O. Nielsen, A. Pieringer, W. Kropp, W. Zhai, Calibration and validation of the dynamic response of two slab track models using data from a full-scale test rig, Engineering Structures 234 (2021) 111980.